JLCX-005
Jan. 2003

JLC X-BAND TECHNICAL NOTE

First HDDS cell fabrication for replacing middle part of H60VG3N

T. Higo, Y. Funahashi, Y. Higashi, N. Hitomi , N. Kudoh, T. Kume, Y. Morozumi, K. Takata, T. Takatomi, N. Toge and Y. Watanabe

* KEK, High Energy Accelerator Research Organization
1-1, Oho, Tsukuba, Ibaraki, 305-0801, Japan

Abstract

Six 45mm diameter HDDS cells were fabricated to replace the middle part of H60VG3N structure for investigation of high-field performance of the slotted cells. This report was written for serving the necessary information to analyze the high-field performance of these cells. One of the key issues in this fabrication is how to suppress the local surface field enhancement, both electric field and magnetic one in a slotted cell, which stems from the discontinuity of surface tangential plane. Firstly we review some of the specifications in this respect, especially stressing the intersection between the milled surface and the turned one followed by the description of the fabrication processes. Then the maximum-possible evaluation and/or estimation of the mechanical characteristics of the produced cells is described though we understand that we have not reached the well-established process by the time of this actual fabrication. The electric characteristics of the cells were also measured and described. Finally, we discuss some of the existing problems and possible improvements for future fabrication.

1. Introduction

JLC/NLC linear collider main-linac accelerator structure composes of the radially-slotted cells with varying geometry from cell to cell and it should be operated at a very high field, E_{NL}=65MV/m. Recent high power tests at SLAC showed frequent soft breakdowns near input coupler wave guide iris [1]. One of the possible causes is speculated to be the surface temperature rise of a few hundred degrees Celsius within a pulse of 400nsec[2]. A structure, T53VG3MC, was designed to suppress the temperature rise at this input coupler by removing the iris with using mode converter design as the coupling mechanism between the wave guide to the accelerator guide. The structure was conditioned without soft breakdowns in the input coupler region, suggesting the proof of the cure due to low surface magnetic field. Since the JLC/NLC structure cells are equipped with slots and manifolds, the local maximum surface magnetic field necessarily enhances by a factor of square root of 2 so that the resultant surface temperature rise becomes twice comparing the cells without slots and manifolds. Therefore, further enhancement of the surface magnetic field should be suppressed.

A quick test was planned as of ISG8 to high-power test such cells[3]. To this end, six cells at the middle part of the H60VG3N structure were replaced by the corresponding HDDS cells, which are the cells of the present paper.

Firstly, a general description of the cells is made focusing to the characteristics of the junction between two surfaces. Then the actual mechanical specifications for these cells are described. Secondly, are presented some key ideas on the fabrication processes. Then, the evaluation of the mechanical characteristics of the test cells and the production-version cells is made followed by the electrical measurement. Finally, we discuss some of the existing problems and ideas for future improvements.

2. Cell shape and specifications

A part of the KEK drawing (HDDS0-1000-034-02) of the present HDDS cells is shown in Fig. 1. As the nominal fabrication method of this cell, we assume the turning operation with lathe for the area, which is cylindrically symmetric with respect to the beam axis while all other 3D shapes are milled with its spindle rotation axis always parallel to the beam axis. In Fig. 2 is shown the surface magnetic field distribution from lower field with blue color to higher field with red color. These red-colored regions are the points where we tried to make smooth junction between two kinds of surfaces.

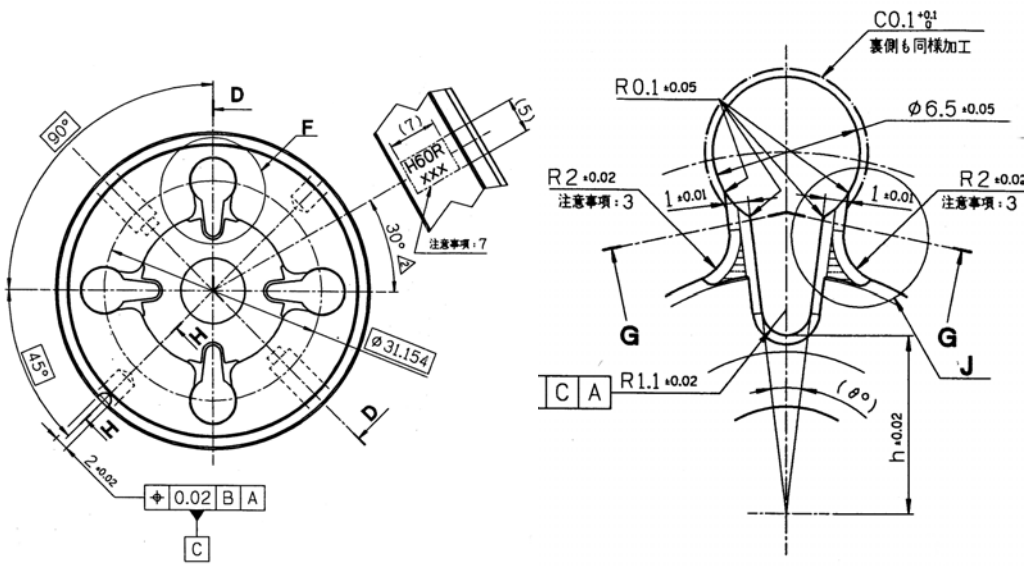

(a) (b)

Fig. 1 HDDS cell shape (a) plan view and (b) close-up of slot and manifold.

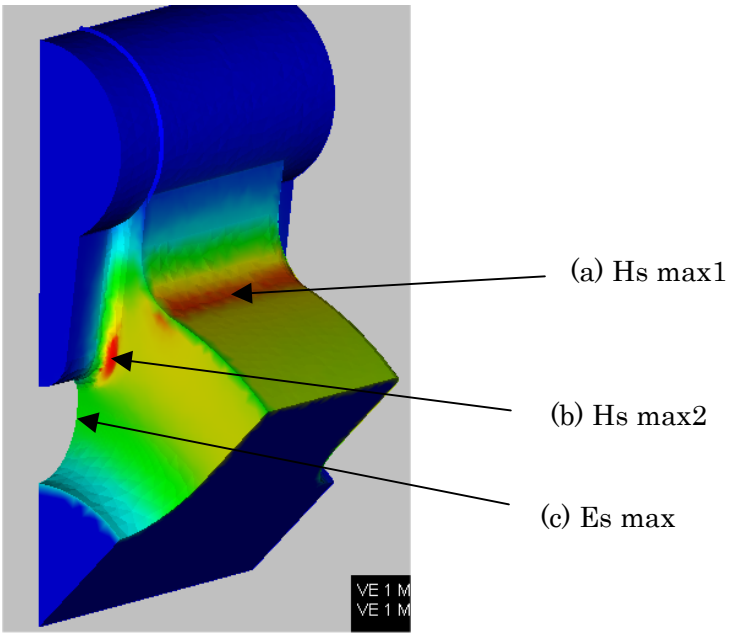

Fig. 2. Surface magnetic field (Hs) distribution. Red is highest region.

Frequency requirements and related tolerances:

The tolerances of the relevant dimensions were determined to make the cells within the tuning range of the dimple tuning ±20MHz. Based on very rough or even intuitive estimation, we used the

following sensitivities,

$\delta F/\delta b = -1 MHz/\mu m$,

$\delta F/\delta a = 0.5 MHz/\mu m$,

$\delta F/\delta p = 0.2 MHz/\mu m$,

$\delta F/\delta W = 0.2 MHz/\mu m$,

where “F” is the frequency, “b” the cell radius, “a” beam hole radius, “p” cell length and “W” the width of slots and the width of pathways from cell to manifold, where both widths changes by the same amount[4]. Since we specify the mechanical tolerances as

$\delta b = \pm 10 \mu m$,

$\delta a = \pm 10 \mu m$,

$\delta p = \pm 10 \mu m$,

$\delta W = \pm 40 \mu m$,

we simply estimate the maximum error propagation as

$$\Delta F = |(\delta F/\delta b)\, \delta b| + |(\delta F/\delta a)\, \delta a| + |(\delta F/\delta p)\, \delta p| + |(\delta F/\delta W)\, \delta W|$$
$$= 10+5+2+8 = 25 MHz.$$

This value is a little larger than the above tuning range. However, we think the present tolerance specification is practical because of the following consideration. At first, most sensitive dimensions, “b” and “a”, are positively correlated in many cases to cancel the frequency error. Secondly, even the positioning error of slots and the associated width errors of the opening to manifold are large, the average width error is small because the relative positioning of the slots among each other in a cell are much more precise than the above mechanical specifications. Finally, even the tuning range can be enlarged if really necessary after additional annealing[5].

Requirement of tangential surface discontinuity:

One of the most difficult fabrication processes we encountered is the mutual positioning of the turning and milling. If two independent surfaces are made with poor mutual positioning, it often makes a ridge between them. Therefore, the surface magnetic field, which climbs over the ridge enhances the surface current which flows along the ridge. Two places of our most concern, shown in Fig. 2, are (a): “2b—r2” that between the turned cylindrical surface of a cell diameter and the milled cylindrical wall with its radius 2mm and (b): ”r0.5—flat” that between the turned part of a cell flat end and the rounding with a radius of 0.5mm along the rim of the slot. Considering the estimation that the surface magnetic field on the coupler iris enhances linearly on the turning angle comprising each chamfer. The estimation with the typical mesh size of 5 microns gives 50% enhancement if the angle is 5 degrees[6]. Since we do etching for 1 minute on the cells removing about 3 microns, the 5 micron order of rounding is considered reasonable supporting the used mesh size. Thinking these, we specified the tangential discontinuity at (a) “2b—r2” as

(a) “2b—r2” < 5 degrees.

The requirement on the position (b) “r0.5—flat” might be severer because the highest point is near the maximum point in the surface electric field[2]. However, the area is small and may not be so serious. At least we do not have any better guidance on the requirement so that we specified

(b) “r0.5—flat” < 12 degrees

intuitively in addition to considering the perspective on the development within a limited period based on the present fabrication status.

Another part (c) is along a circle, where the elliptical beam hole and the cell flat surface meet. The electric field is rather high though not the highest point on the elliptical shape. We specified the tangential discontinuity as

(c) “ellipse—flat” < 1 degree.

Since this part is made only by turning, any problem does not arise as long as the turning is precise enough. However, the company who made the present cells uses a medium-precision turning lathe, typically used for the work for ten micron precision. Because we suffered from some troubles, we specified to keep this in mind.

3. Fabrication method

Based on the vendor’s feasibility and considering the above requirements, we set the fabrication as described below.

Fabrication steps:

The basic procedure of the fabrication of the cells is the following.

1. Cut disk from bar stock
2. Rough turning
3. Medium machining
4. Annealing at 500C for 1 hour procedure
5. Boring tuning holes
6. Milling of cup side
7. Milling of disk side
8. Turning cup-side end surface
9. Turning disk-side end surface and cell inside till “2a” point
10. Rinsing in an isopropyl-alcohol bath with ultra-sonic vibration
11. Drying by blowing with nitrogen gas

Tools and machining conditions:

The poly-crystal diamond tool with its radius 0.2mm was used for turning. The turning lathe is made by Mori-Seiki co. Disks are chucked at outside diameter with soft jaws with as less a pressure as possible.

The rounding of slot rim was performed using a ready-made shaped tool made of carbide, whose shape is shown in Fig. 3. Escape angle is 3 degrees with radial extension by 50μm. The corresponding control in spindle axial direction is required to be within 14μm to keep the tangential-discontinuity angle less than 5 degrees. The cup-side rounding is made on the finished turned surface, while the disk-side rounding is on the surface with 10 micron undercut. The disk-side undercut is due to the required final finish to make the end surface flat by removing the local bumps created by milling near manifold. Though this is for making the flat surface for diffusion bonding, this final turning is made on all of the disk-side surface because stopping near "2b" is not good considering the poor lathe positioning. The final cut on cup-side is applied only on end surface because of the natural separation from cell inside by geometrical shape.

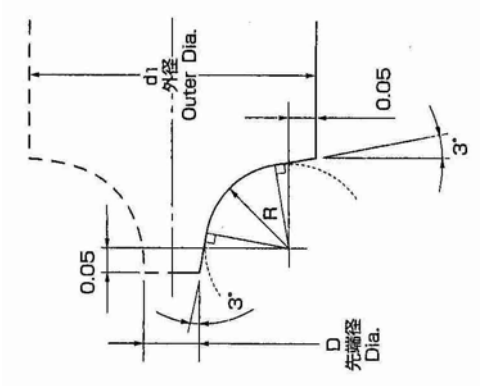

Fig. 3. Milling tool

Cutting fluid and rinsing at vendor company:

Cutting fluid both for turning and milling is Idemitsu-Kosan DAFNI-CUT GC-30, which contains Clorine (2.45wt%) and Sulfer (0.5wt%). Cells are rinsed in an isopropylalcohol bath with ultrasonic vibration. They are wrapped in a clean paper and sent to KEK.

Process to form the junction (a):

The junction is designed to make at the intersection between turning at radius "b" and the escaping route of the milling tool along a specified path as shown in Fig. 4. The milling tool path on the cylinder with radius 2mm towards the manifold removes before reaching to the tangential point by 3 degrees. Its contour shapes a circle of the radius of 3mm. This small radius is thought to be good for removing the scissel easily near the junction point. If the relative positioning of turning and

milling is not perfect, we expect the intersection at different points. The resulting tangential discontinuity is plotted as a function of the distance of two circles, “2b” and “r=2mm”, as shown in Fig. 5. Blue line shows the case intersecting with a circle “r2”, while red one the case with an escaping circle with r=3mm and the green one the case intersecting with a line, though the last was not adopted in the present case. As shown in the figure, the positioning should be between -6μm and +4μm with respect to the ideal case in order to suppress the discontinuity within 5 degrees, as specified. This is fairly tight comparing to the specification of the turning where δb=±10μm and the milling positioning of the order of a few tens of μm. Therefore, we are NOT certain that the present machining satisfies the requirement. The case escaping along a tangential line at 3 degrees was not adopted worrying about the scissel point of view.

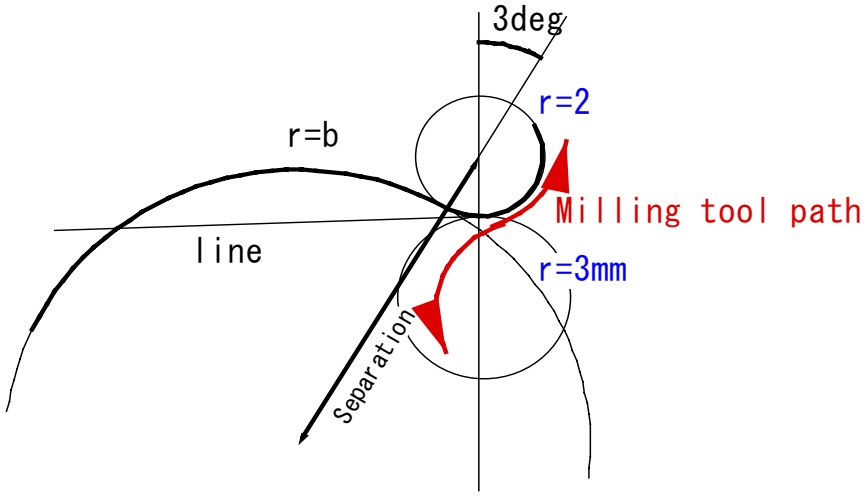

Fig. 4. Milling tool path shown in red line for “2b—r2”.

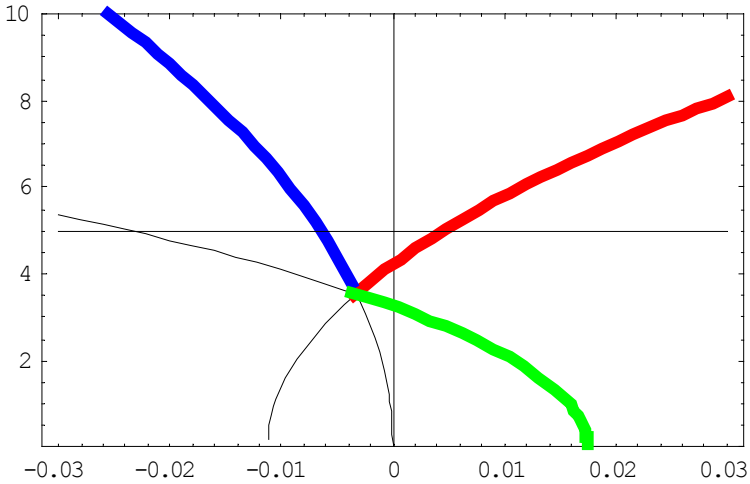

Fig. 5. Dependence of tangential discontinuity at “2b—r2” on relative positioning error between turning and milling.

4. Results on mechanical characteristics of cells

Flatness and parallelism:

Flatness is inspected by CMM on 18 points over each end surface. One of the typical results is shown in Fig. 6. As shown in the figure, the flatness and parallelism of the present HDDS cells are a few microns.

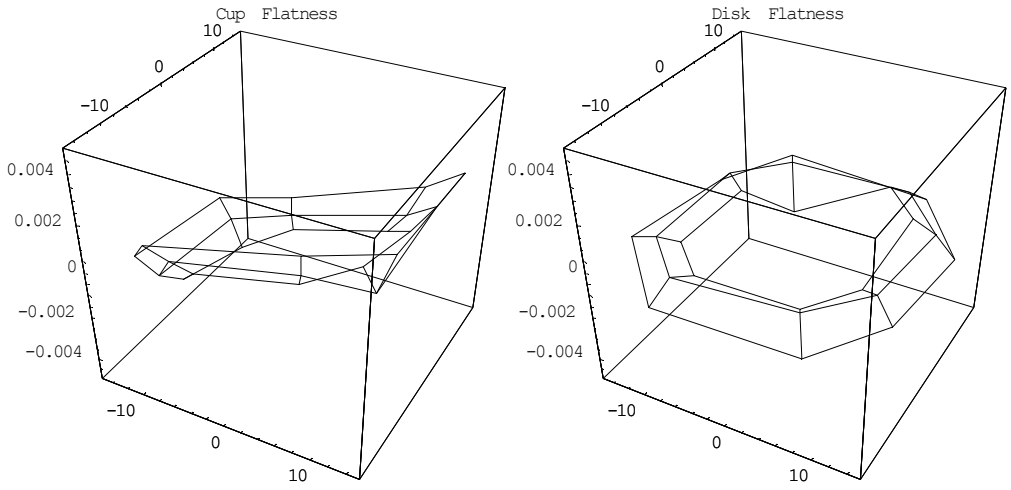

Fig. 6. Flatness of a typical disk.

Surface roughness:

Surface roughness was measured by using a Formtracer[7] with diamond-stylus of ϕ5μm at 5mN force on test cells. Typical results are shown in Fig. 7. The upper trace is on the elliptical surface while the lower trace on the flat surface. The former smooth waving is due to the tool shape, confirmed by the completely symmetric pattern at both sides of the thin disk with thickness "t" with respect to the "2a" position. Removing this waviness, the roughness of the turning surface is about Ry=1.4μm, a little larger than spec. of 1μm, while that of the latter Ry=0.4μm much better than spec.

Typical example of the roughness of milled surface for shaping a radius of 0.5mm is shown in Fig. 8, presenting the residual from the fit circle. The measured roughness is Ry=1.5μm.

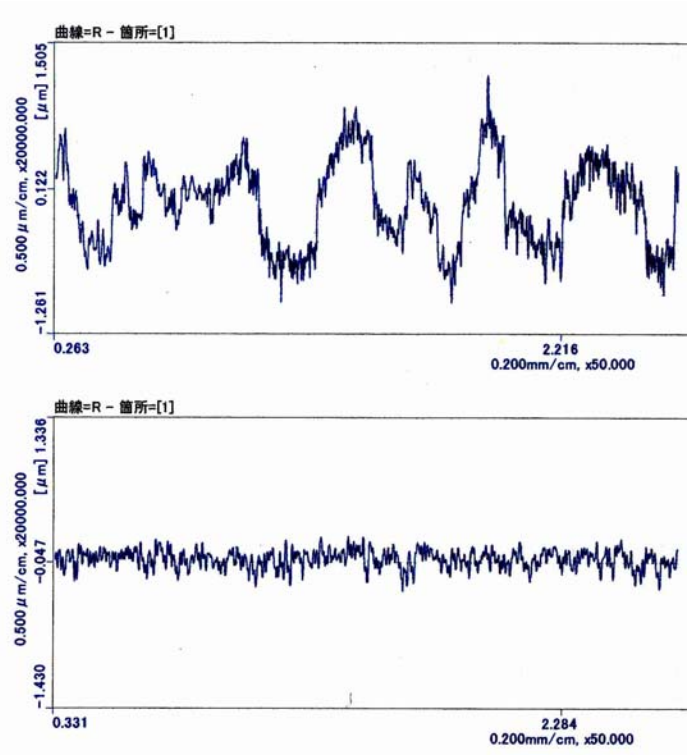

Fig. 7. Roughness of turned surface. Upper is on elliptical shape while lower at a flat part.

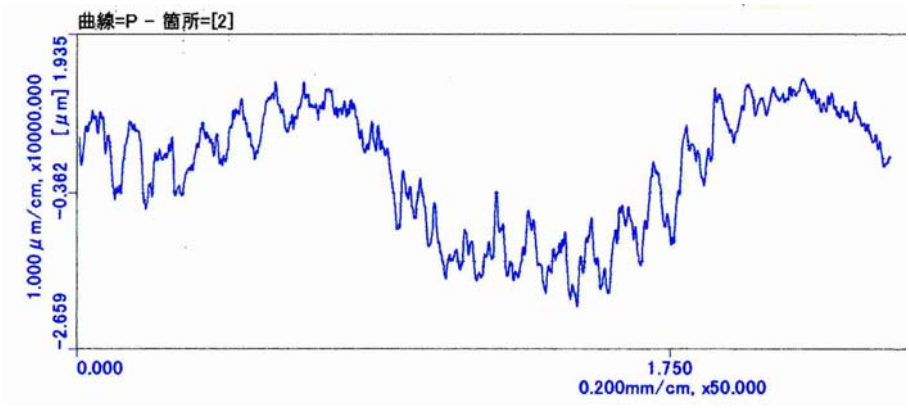

Fig. 8. Roughness of milled surface on radius 0.5mm.

Tangential discontinuity:

The discontinuities of the tangential plane between two surfaces are measured with using a Formtracer[7].

Typical example of (a) “2b—r2” is shown in Fig. 9. Lower figure shows the whole contour from one of the “r2” connecting to “2b” and reaching to another “r2”. Upper two figures are those of the expanded view with manually fit with lines, reading the intersection angles of 9 and 11 degrees, much larger than the specification of 5 degrees. Typical reading/fitting error is about 5 degrees or less. Because this measurement can only be performed by cutting the disk into half, we did not

measure the actual cells but only speculate from the examples in the test cells. From all of the measured test cell result, we should admit that the angle of 15 degrees or so will appear at (a) "2b—r2" in the actual production cells.

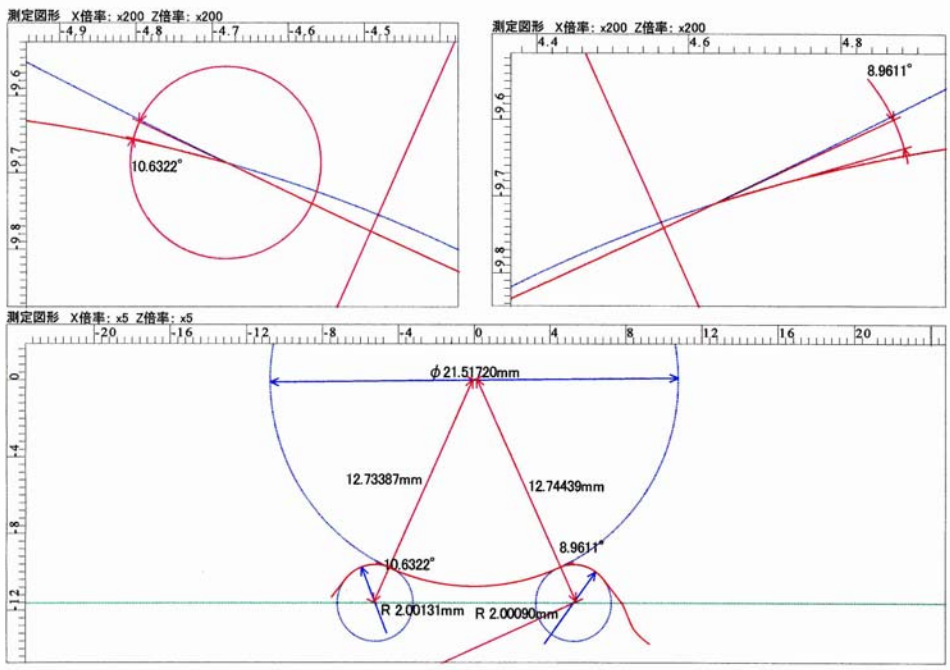

Fig. 9. Intersection at (a), "2b—r2".

We also used the same equipment to measure the intersecting angle (b) "r0.5—flat". Typical result is shown in Fig. 10. This example shows the profile from ellipse (lower-right) through r0.5 (top) to slot wall (left). The most important point is measured as 9 degrees here. The intersection on the left side of this example is not very critical so that we did not pay much attention on the intersecting angle at left side. Since we were afraid of perturbation due to the measurement on the actual cells, we did not measure the angle for actual cells so that we can simply estimate from the measured test cell results. Collecting the results on all of the measurement on test cells, we estimate that this angle will be between 5 to 20 degrees in the actual production cells.

The discontinuities at (c) "ellipse—flat" are also checked. As long as the point is shaped by turning in a continuous cutting without combination of two spurs, the measured angles are less than 2 degrees.

Summarizing the above results, the estimation of the discontinuities for the production cells is listed in Table 1.

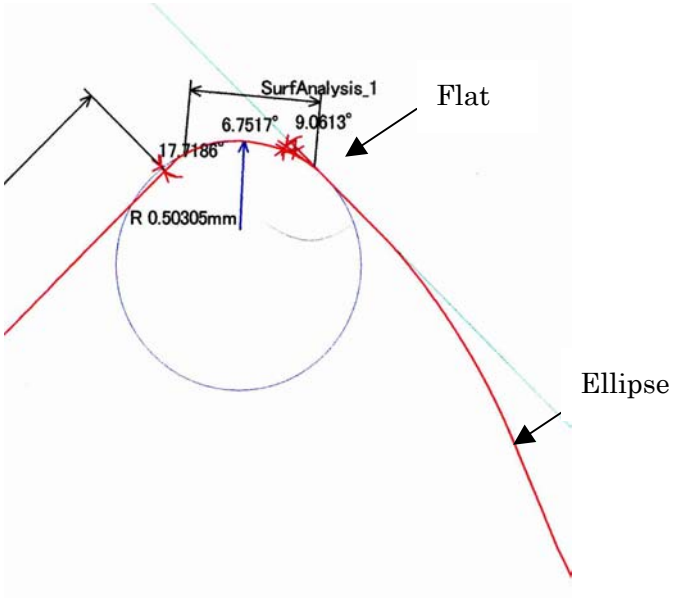

Fig. 10. Intersection at (b), “r0.5—flat”.

Table 1. List of estimated angle discontinuities in actual production cells.

Place	Specification	Estimation in production cells
(a) “2b—r2”	< 5°	3—15°
(b) “r0.5—flat”	< 12°	5—20°
(c) “ellipse—flat”	< 1°	0—2°

Dimensions of actual cells:

The important dimensions of the actual production cells were measured by CMM (ZEISS, UPMC CARAT 850) at KEK in addition to the measurement by the vendor company. The KEK CMM values suffer from the indentation by probe into the copper surface by an amount of 1—2 micron depth. The probe diameter varies from 1mm to 3mm with pressure of 0.2N. The results shown below do not take the indentation into account.

Diameters are shown in Fig. 11. Scattering in diameter is small though “2a” is much larger than nominal, almost at the edge of the tolerance by taking the indentation correction into account. The “2b” are precise within ±5μm. Thickness is shown in Fig. 12. We realized that the thickness was not well controlled but we accepted because it does not perturb frequency much nor give rise any difficulty in high field operation.

Key dimensions, which are shaped by milling cut, are shown in Fig. 13. As shown in the figure, the parameter “h”, the positioning of the slots, are very precisely controlled, indicating the capability of the vendor company which usually produces precision jigs and tools in a micron

accuracy. The W1 and W2 are the average width of four slots at the radius r=”b” and r=”b-2”, which are measured to inspect the slot frequency error. This is found to be controlled within 10 microns. The W3 is the width of a channel between two walls connecting cell and manifold with height “p-t”. Three points are measured on each cylindrical wall to estimate the center and radius of the cross-sectional circle and calculate the distance of the two circles to obtain W3. W3 is found to be controlled within 15 microns.

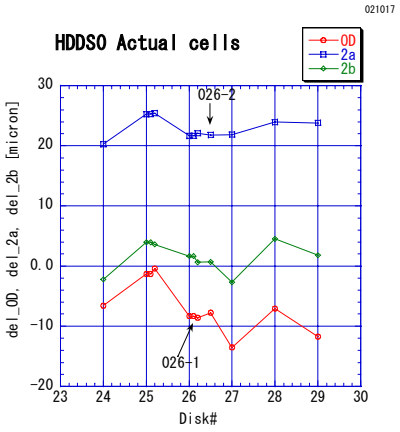

Fig. 11. Diameters of actual cells.

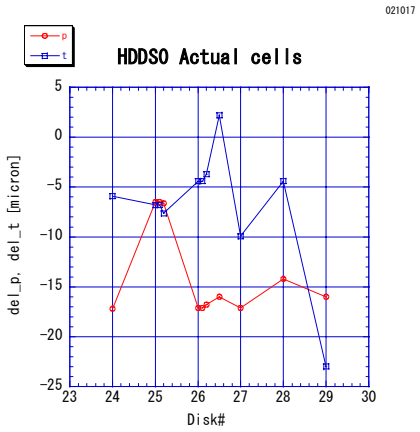

Fig. 12. Thickness of actual cells.

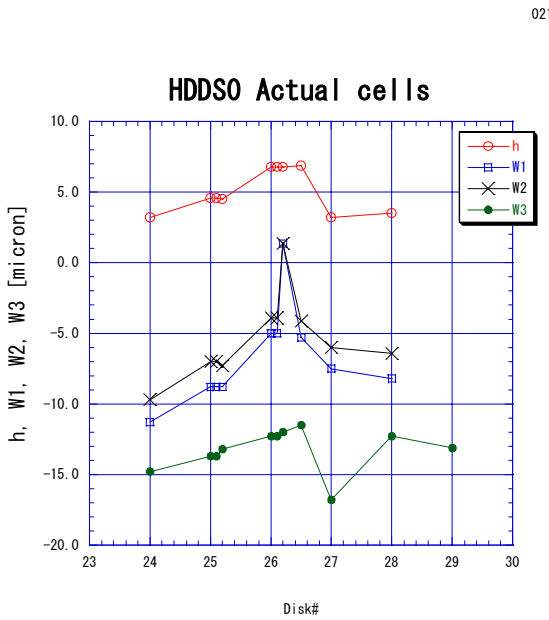

Fig. 13. Width dimensions associated with slots shaped by milling.

5. RF measurement result

RF test characteristics:

Half cells and half cylinder were made in the same manner as that for actual cells. These two parts were assembled to make two half cells to measure Fπ mode. The result is shown in Fig. 14, where no saturation in frequency nor Q value was obtained even at the maximum available force of 350kg on nominal surface of ca. 750mm^2, pressure of about 0.5kg/mm^2. We speculate from the frequency saturation curve that the measured frequency at the maximum pressure gives 1—2 MHz lower frequency than actual. This error is much smaller than the tuning range so that we did not try to apply more force than the present maximum.

Fig. 15 shows the Fπ frequency versus the rotational misalignment between half disk and half cylinder. We try to set the disks in the following measurement of actual cells with adjusting the rotational alignment notch by eye at the outer rim of ϕ45mm. Since we can set the disks within ± 0.2mm among each other, we expect the frequency error due to the rotational misalignment of disks of± 1MHz or less.

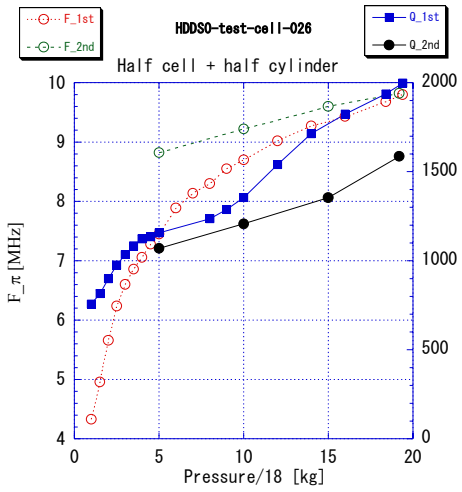

Fig. 14 Frequency characteristics versus mechanical pressure.

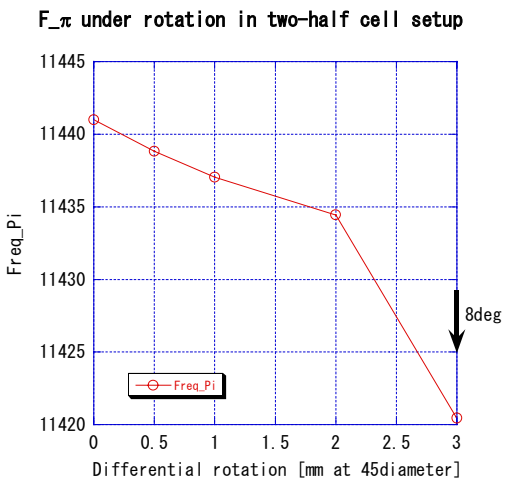

Fig. 15. Frequency shift due to relative rotation between half cells.

Frequency scattering:

Each cell of number #26 was sandwiched by half disk and half cylinder to measure F0 and Fπ mode frequencies. Results are shown in Fig. 16. We cannot deduce any clear estimation of their dimensional information but the cell frequencies are within ±5MHz, assuming the twice error values than the measurement scattering in Fig. 16. If we read the mechanical dimensional errors as

$\delta 2a = \pm 2\mu m$

$\delta 2b = \pm 4\mu m$

$\delta 2p = \pm 10\mu m$

$\delta W = \pm 3\mu m$,

the rms value in frequency error becomes ± 2.5MHz, while simple summation of the errors become ± 5MHz. These values are roughly considered to be consistent to the measured frequency scattering.

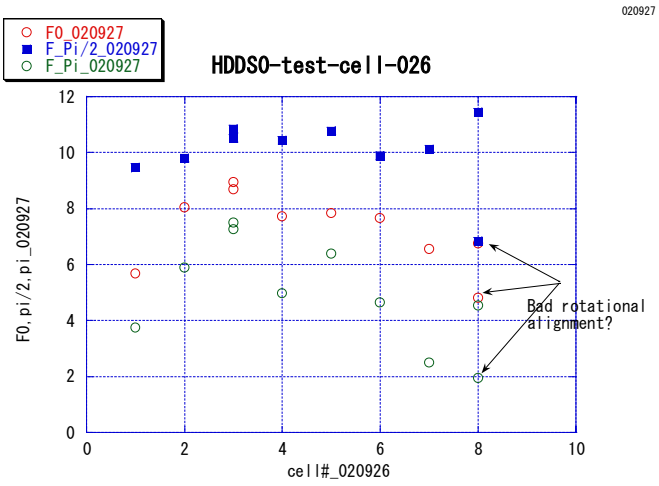

Fig. 16. F0 and Fπ mode frequencies of test disks #26.

Absolute frequency estimation:

In order to get the absolute frequency of 5π/6 mode from stack measurement with a limited number of disks, we observed the dispersion curve of each setup. Each curve was fit with a functional form

$A + B\,\mathrm{Cos}(\theta) + C\,\mathrm{Sin}(2\theta)$,

where θ is the phase advance per cell and A, B and C are the fit variables. Fittings are shown in Fig. 17 and the obtained 5π /6 mode frequencies are shown in Fig. 18. Then the frequency at $N \rightarrow \infty$ is obtained as 11423.7MHz. This value is corrected to estimate that at 45C in vacuum in an actual setup as follows;

Nitrogen atmosphere → vacuum +3MHz

Measurement at 23C → operation at 45C -4MHz

Identical disk setup → actual setup in a structure with varying dimension +5MHz

Summing all of these corrections makes the final estimation of the absolute frequency of the cells at about 11428MHz. It should be noted that the above third correction comes from the design tuning of "b" of the actual cell which is larger than the nominal value taking into account the averaging procedure when converting from original "disk" design (center disk sandwiched by two identical

half cylinders at both ends) to “cup” design (actual design, full cylinder + disk at one end)[8].

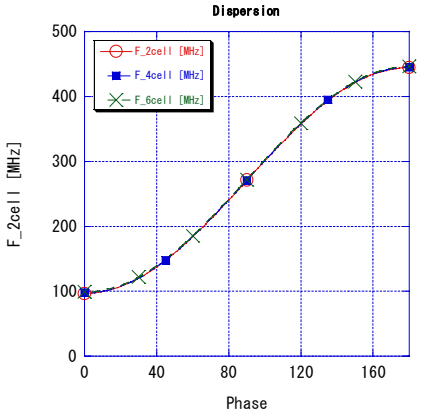

Fig. 17. Dispersion curve measurement on setups with three different numbers of disks.

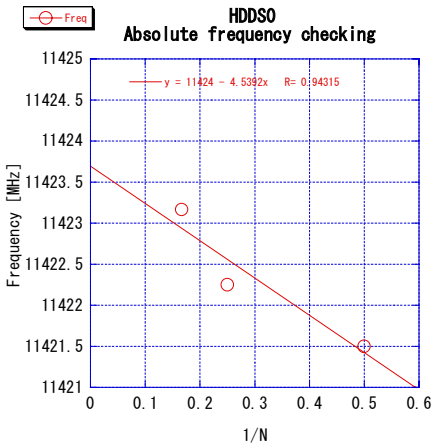

Fig. 18. 5π/6 mode frequency as function of 1/N(number of cells).

6. Possible improvements in future for existing problems

We recognized many difficulties through the fabrication of the present HDDS cells. In the following are listed some possible cures to suppress them.

1. Usage of better turning lathe with chucking with less deformation, probably vacuum chuck
   This is particularly for obtaining good surface flatness to make a better positioning in a milling stage, in addition to get flat end surface good for diffusion bonding.
2. Milling tool escape path with a larger radius
   Since the relative positioning between “2b” turning and “r2” milling is too severe to keep the specified discontinuity angle, the escape circle radius should be close to “b” as long as the scissel does not give any severe scratches on surface.
3. Milling tool for chamfering slot rim with a radius 0.5mm with a steeper escape angle
   Since the depth positioning of the tool with respect to the turned surface is tight, the escape angle of the tool should make larger to an angle a little less than tolerable discontinuity angle.

We should note that the criteria on discontinuity of tangential plane should be revisited after studying the high-field performance of the present cells.

7. Acknowledgments

This program is under the collaboration between SLAC and KEK on linear collider research and development. We greatly owe in many of theoretical investigation and discussions to our colleagues at SLAC. We thank MORIKAWA Co. LTD. for rather open discussions with KEK in many stages of the R&D and actual production.

8. References

1. C. Adolphsen, ISG8, SLAC, June 2002.
2. V. Dolgashev, ISG9, KEK, Nov. 2002.
3. J. Wang, Summary of ISG8, SLAC, June 2002.
4. Y. Morozumi, Private communication.
5. J. Wang, Private communication.
6. T. Higo, NLC Collaboration meeting, SLAC, Nov. 2002.
7. Mitsutoyo co. ltd., Formtracer CS-5000.
8. Z. Li, ISG8, SLAC, June 2002.